for Ni and Pd. As mentioned above, the Au-MILC annealing temperature has been set higher than the Au-Si eutectic temperature and results in a liquid phase which will enhance the diffusion of Si atoms and results in longer MILC lengths. However, the eutectic temperatures of Ni and Pd are 964 and 782°C which are higher than the annealing temperatures in the MILC process and no liquid phase will be found. Therefore, for a given time, the MILC length is short. The MILC rates obtained for Au inducement were decreased from 15.9μm/h to 12.3μm/h with extended annealing treatment from 10 to 40h. This phenomenon has been reported due to the continuous rearrangement of the atoms in the a-Si during the long annealing treatment [5], thus slowing the MILC rate. Compared with Ni and Pd, Au shows more characteristics that are preferable for low temperature poly-Si TFT fabrication, especially the large reduction in thermal budget due to the increased MILC rate. These are the key points for the development of the low cost ICs on conventional glass substrates.

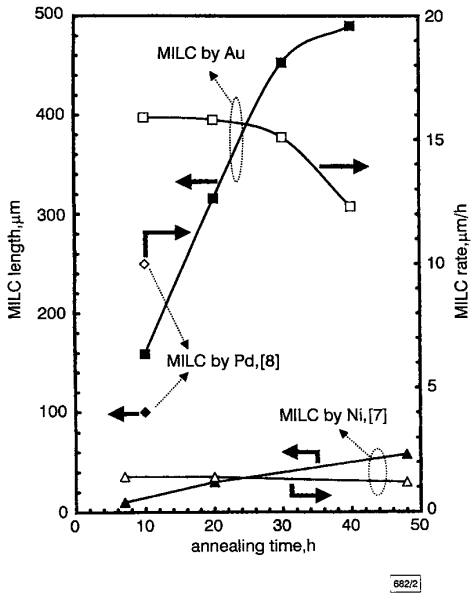

Fig. 2 *Dependence of MILC length and rate on annealing treatment time*

Flow rate of H_2 is set at 60sccm and annealing temperature is 400°C

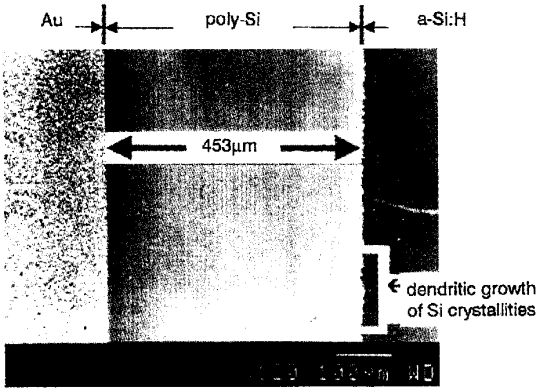

Fig. 3 *SEM photograph of lateral crystallisation of a-Si:H films induced by Au*

a-Si:H films were deposited with H_2 flow rate of 60sccm and then annealed at 400°C for 30h

The quality of the Au-MILC film was examined by SEM analysis, as shown in Fig. 3. The a-Si:H film was deposited on an oxidised c-Si substrate with an H_2 flow rate of 60 sccm and then annealed at 400°C for 30h. From the Figure, we can see that the MILC film has been crystallised homogeneously. In addition, the dendritic growth of Si crystallites by Si atom diffusion is clearly observed at the boundary of the poly-Si/a-Si thin film.

Conclusion: By annealing at 400°C, a-Si:H film realised by Au inducement shows a very high crystallisation rate (15.1 – 15.9μm/h) and MILC lengths longer than 159μm can be obtained for a times > 10h. The preferable characteristics are attributed to the lower Au-Si eutectic temperature forming a liquid phase for Si atom diffusion. Based on the work in this Letter, MILC by Au inducement has been shown to be a suitable technology for the low temperature fabrication of poly-Si TFTs on glass substrate for low cost IC applications.

Acknowledgment: The authors acknowledge the financial support from the Science Council of ROC under contract of NSC 88-2215-E-006-008.

20 April 1999
Electronics Letters Online No. 19990743
DOI: 10.1049/el:19990743

K.H. Lee, Y.K. Fang and S.H. Fan (*VLSI Technology Laboratory, Department of Electrical Engineering, National Cheng Kung University, Tainan, Taiwan, Republic of China*)

References

1 LEE, S.W., and JOO, S.K.: 'Low temperature poly-Si thin-film transistor fabrication by metal-induced lateral crystallization', *IEEE Electron Device Lett.*, 1996, **17**, (4), pp. 160–162
2 LEE, S.W., IHN, T.H., and JOO, S.K.: 'Fabrication of high-mobility *p*-channel poly-Si thin film transistor by self-aligned metal-induced lateral crystallization', *IEEE Electron Device Lett.*, 1996, **17**, (8), pp. 407–409
3 BHAT, G.A., JIN, Z., KWOK, H.S., and WONG, M.: 'Effects of longitudinal grain boundaries on the performance of MILC-TFT's', *IEEE Electron Device Lett.*, 1999, **20**, (2), pp. 97–99
4 AOYAMA, T., KAWACHI, G., KONISHI, N., SUZUKI, T., OKAJIMA, Y., and MIYATA, K.: 'Crystallization of LPCVD silicon films by low temperature annealing', *J. Electrochem. Soc.*, 1989, **136**, (4), pp. 1169–1173
5 JIN, Z., MOULDING, K., KWOK, H.S., and WONG, M.: 'The effect of extended heat treatment on Ni induced lateral crystallization of amorphous silicon thin films', *IEEE Trans.*, 1999, **ED-46**, (1), pp. 78–82
6 LEE, S.W., JEON, Y.C., and JOO, S.K.: 'Pd induced lateral crystallization of amorphous Si thin films', *Appl. Phys. Lett.*, 1995, **66**, (13), pp. 1671–1673
7 HULTMAN, L., ROBERTSSON, A., and HENTZELL, H.T.G.: 'Crystallization of amorphous silicon during thin-film gold reaction', *J. Appl. Phys.*, 1987, **62**, (9), pp. 3647–3655

Demonstration of efficient p-type doping in $Al_xGa_{1-x}N$/GaN superlattice structures

I.D. Goepfert, E.F. Schubert, A. Osinsky and P.E. Norris

Enhanced acceptor activation, reduced acceptor binding energy and enhanced conductivity are demonstrated in $Al_xGa_{1-x}N$/GaN doped superlattice structures. An acceptor activation energy of 58meV is demonstrated in an $Al_{0.20}Ga_{0.80}N$/GaN superlattice structure with a period of 200Å. This value is significantly lower than the 200meV activation energy measured in bulk GaN. The dependence of activation energy on the Al content of the superlattice is consistent with that predicted by the theoretical model. The demonstration of improved p-type doping characteristics in GaN is expected to enable the realisation of electronic and optoelectronic devices with improved properties.

The GaN material family exhibits a large acceptor binding energy which has been determined to be 200 ± 50meV [1 – 3]. The large acceptor binding energy is in reasonable agreement with the hydrogenic model for effective-mass-like acceptors in GaN, which predicts an activation energy of 130meV. The large acceptor binding energy leads to a very low activation of acceptors in GaN, and, consequently, to low p-type conductivity in devices such as LEDs, lasers, and bipolar transistors. Much research is devoted to the search for a shallow acceptor in GaN but no shallow acceptor has yet been found [4, 5].

It has been proposed that superlattice doping can reduce the acceptor activation energy and lead to a higher activation of acceptors in $Al_xGa_{1-x}N$/GaN doped superlattice structures [6]. The concept of doped superlattice structures is illustrated in Fig. 1. The bandgap of a one-dimensional $Al_xGa_{1-x}N$/GaN superlattice structure varies periodically along one spatial dimension, as shown in Fig. 1. The superlattice is doped with a constant doping concentration N_A. If the acceptor energy level follows the valence band edge, acceptors residing in the Al-rich regions of the superlattice are likely to become ionised by tunnelling rather than by thermal activation. As a consequence, the fraction of ionised acceptors is much higher in doped superlattice structures as compared to homogeneous GaN.

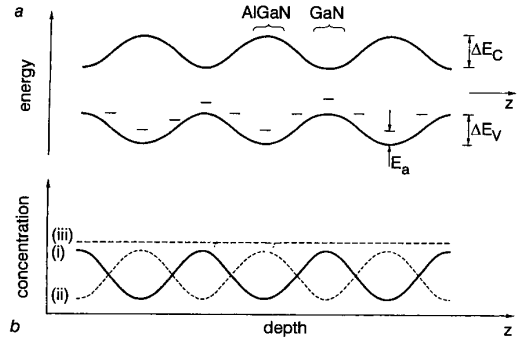

Fig. 1 *Schematic diagrams of superlattice structure and concentrations*

a Schematic band diagram of $Al_xGa_{1-x}N$/GaN doped superlattice structure
b Schematic illustration of free hole concentration (p), ionised acceptor concentration (N_A^-), and acceptor concentration (N_A)
(i) P
(ii) N_A^-
(iii) N_A

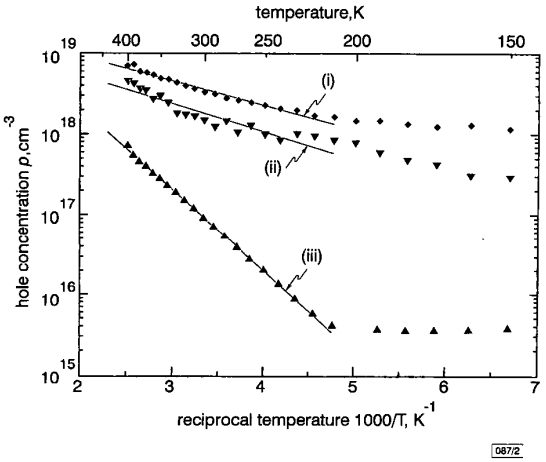

Fig. 2 *Free hole concentration against reciprocal temperature for $AlAl_xGa_{1-x}N$/GaN doped superlattices with x = 10 and 20% aluminium content as well as carrier concentration in p-type bulk GaN sample*

(i) E_a = 58meV ($Al_{0.20}Ga_{0.80}N$/GaN)
(ii) E_a = 70meV ($Al_{0.10}Ga_{0.90}N$/GaN)
(iii) E_a = 200meV (p-type GaN)

In this Letter, we present experimental evidence of enhanced acceptor activation, reduced acceptor binding energy, and enhanced conductivity in $Al_xGa_{1-x}N$/GaN doped superlattice structures. The MBE-grown superlattices have 20 periods of GaN (100Å) and $Al_xGa_{1-x}N$ (100Å). The interfaces are not intentionally graded. Samples with two different aluminium contents, namely x = 10 and 20%, are investigated. Good Ohmic characteristics are obtained with 850Å thick unannealed Ni contacts deposited on square-shaped 2.5 × 2.5mm van der Pauw samples used for Hall-effect measurements.

The carrier concentration against reciprocal temperature of the doped superlattice samples is shown in Fig. 2. Both samples (with x = 10% and 20% Al content) have an intentional doping concentration of $N_A \simeq 10^{19}cm^{-3}$. Comparison of the carrier concentration for the two samples reveals that the sample with the higher Al content has the higher carrier concentration throughout the entire temperature range. The band modulation increases with the Al content so that a higher carrier concentration is expected for that sample, in agreement with the theoretical model.

It is found that the acceptor binding energy in doped superlattice structures is reduced as compared to that of bulk GaN. The acceptor binding energy is deduced from the temperature dependence of the carrier concentration using the equation

$$p \propto e^{-E_a/(kT)}$$

where E_a is the acceptor activation energy and kT is the thermal energy. Activation energies of 70 and 58meV are obtained for superlattices with 10 and 20% Al content, respectively. A linear least-square fit to the experimental data is used in the temperature range 200 to 400K. The dependence of the acceptor binding energy on the Al content of the superlattice is consistent with that predicted by the theoretical model [6] and is also consistent with more detailed calculations [7]. The data shown in Fig. 2 also reveal a 200meV acceptor binding energy for a homogeneous p-type GaN.

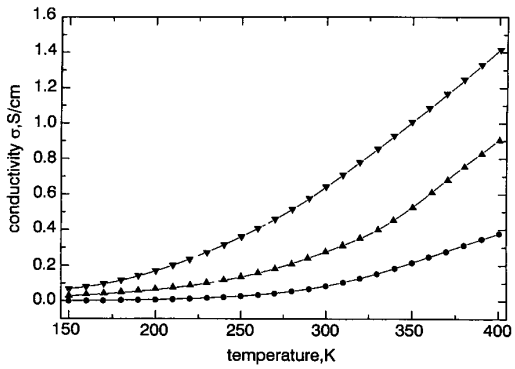

Fig. 3 *Conductivity against temperature for $Al_xGa_{1-x}N$/GaN doped superlattices with x = 10 and 20% aluminium content and p-type bulk GaN sample*

▼ p-type $Al_{0.20}Ga_{0.80}N$/GaN superlattice
▲ p-type $Al_{0.10}Ga_{0.90}N$/GaN superlattice
● p-type GaN

The conductivity of the $Al_xGa_{1-x}N$/GaN superlattices against temperature is shown in Fig. 3. The hole mobility of both superlattices at room temperature is 1.1–1.2cm²/Vs. The hole mobility has a weak temperature dependence. Inspection of Fig. 3 clearly reveals that the conductivity of the superlattice sample with the superlattice with 20% Al content is clearly higher than for the 10% Al content superlattice. We note that this is the opposite trend to that observed in bulk $Al_xGa_{1-x}N$ [8, 9]. Thus the results reported here will not only be beneficial to GaN, but also to the $Al_xGa_{1-x}N$ material system where high p-type conductivity is important as well.

In summary, we present experimental evidence that $Al_xGa_{1-x}N$/GaN doped superlattice structures have enhanced acceptor activation, reduced acceptor binding energy, and enhanced conductivity as compared to bulk GaN. Acceptor activation energies of 70 and 58meV are demonstrated in $Al_{0.10}Ga_{0.90}N$/GaN and $Al_{0.20}Ga_{0.80}N$/GaN doped superlattice structures, respectively. These values are significantly lower than the 200 ± 50meV activation energy measured in bulk GaN. The demonstration of a reduced ionisation energy allows for enhanced conductivity and is expected to result in improved GaN device characteristics.

Acknowledgments: The work at Boston University was supported in part by ONR (C.E.C. Wood) and NSF (R.P. Khosla). The work at NZ Applied Technologies was supported by NSF (D. Gorman, DMI-9760579).

11 May 1999
Electronics Letters Online No: 19990758
DOI: 10.1049/el:19990758

I.D. Goepfert and E.F. Schubert (*Department of Electrical and Computer Engineering, Boston University, Boston, Massachusetts 02215, USA*)

A. Osinsky and P.E. Norris (*NZ Applied Technologies, Woburn, Massachusetts 01801, USA*)

References

1 FISCHER, S., WETZEL, C., HALLER, E.E., and MEYER, B.K.: 'On p-type doping in GaN – acceptor binding energies', *Appl. Phys. Lett.*, 1995, **67**, pp. 1298–1300
2 GÖTZ, W., JOHNSON, N.M., WALKER, J., BOUR, D.P., and STREET, R.A.: 'Activation of acceptors in Mg-doped GaN grown by metalorganic chemical vapor deposition', *Appl. Phys. Lett.*, 1996, **68**, pp. 667–669
3 RONNING, C., CARLSON, E.P., THOMSON, D.B., and DAVIS, R.F.: 'Optical activation of Be implanted into GaN', *Appl. Phys. Lett.*, 1998, **73**, pp. 1622–1624
4 BERNARDINI, F., FIORENTINI, V., and BOSIN, A.: 'Theoretical evidence for efficient p-type doping of GaN using beryllium', *Appl. Phys. Lett.*, 1997, **70**, pp. 2990–2992
5 LEE, J.W., PEARTON, S.J., ZOLPER, J.C., and STALL, R.A.: 'Hydrogen passivation of Ca acceptors in GaN', *Appl. Phys. Lett.*, 1996, **68**, pp. 2102–2104
6 SCHUBERT, E.F., GRIESHABER, W., and GOEPFERT, I.D.: 'Enhancement of deep acceptor activation in semiconductors by superlattice doping', *Appl. Phys. Lett.*, 1996, **69**, pp. 3737–3739
7 GOEPFERT I.D., and SCHUBERT E.F.: Unpublished (1999)
8 TANAKA, T., WATANABE, A., AMANO, H., KOBAYASHI, Y., AKASAKI, I., YAMAZAKI, S., and KOIKE, M.: 'P-type conduction in Mg-doped GaN and $Al_{0.08}Ga_{0.92}N$ grown by metalorganic vapor phase epitaxy', *Appl. Phys. Lett.*, 1994, **65**, pp. 593–594
9 KATSURAGAWA, M., SOTA, S., KOMORI, M., ANBE, C., TAKAUCHI, T., SAKAI, H., AMANO, H., and AKASAKI, I.: 'Thermal ionization energy of Si and Mg in AlGaN', *J. Cryst. Growth*, 1998, **189/190**, pp. 528–531

High room temperature peak-to-valley current ratio in Si based Esaki diodes

R. Duschl, O.G. Schmidt, G. Reitemann, E. Kasper and K. Eberl

Room temperature (RT) *I–V* characteristics of epitaxially grown Si/SiGe/Si $p^+/i/n^+$ Esaki diodes are presented. The incorporation of Ge within the intrinsic (i) zone gives rise to an increased peak current density (j_P = 3kA/cm²) and peak-to-valley current ratio (PVCR) compared to pure Si structures (j_P = 80A/cm²). A detailed investigation and optimisation of post-growth annealing has demonstrated a record PVCR of 4.2 for Si based Esaki diodes.

Semiconductor tunnelling structures exhibiting negative differential resistance (NDR) have been studied intensively for many years. This interest arises mainly from a possible application in high frequency [1] and fast digital devices [2, 3]. Especially in the field of digital circuits, tunnelling structures are a promising way of increasing the performance, density and speed of semiconductor devices [3]. For these devices a high peak current density and a low valley current density are required. These two parameters and the resulting peak-to-valley current ratio (PVCR) are therefore the figures of interest. First measurements on Si Esaki diodes produced by a thermal diffusion process show promising properties but are difficult to reproduce [4]. More control and flexibility is achieved by the use of epitaxial growth methods such as molecular beam epitaxy (MBE). However, owing to difficulties in growing high quality Si layers with very high and abrupt doping profiles, the RT PVCRs achieved so far are no better than ~2 [5, 6].

In this Letter we report the RT *I–V* characteristics of epitaxially grown Si/SiGe/Si interband tunnelling diodes. The samples were fabricated by solid source MBE on Si:p^+ substrates. The doping profiles and the structural quality of the highly doped Si layers were carefully optimised. Low growth temperatures of 460°C for Si:B and 370°C for Si:P were found to provide maximum dopant incorporation with sharp profiles. The investigated structures, suggested by Rommel *et al.* [6], consist of an Si p^+ (3×10^{19}cm^{-3}) buffer layer, followed by a *p*-type δ-doping layer (5×10^{13}cm^{-2}), a 1nm Si/4nm SiGe/1nm Si i-zone, an *n*-type δ-doping layer (1×10^{14}cm^{-2}) and an Si n^+ (5×10^{19}cm^{-3}) cap layer. The δ doping layers cause an enhanced degeneracy of the band structure at the p^+ n^+ junction (see inset of Fig. 1). Therefore, the depletion zone which dominates the width of the tunnelling barrier is reduced, and the tunnelling current increases. At small applied forward voltages, electrons can tunnel from the occupied states in the conduction band (CB) at the *n* side to the empty states below the valence band (VB) at the *p* side. At higher voltages no empty states are available, and the current decreases theoretically to zero. Owing to the thermal current and the excess current, which is a leakage tunnelling current through defect states within the forbidden energy gap, the current increases at higher forward bias [5]. Therefore, a high PVCR can only be achieved by a high tunnelling probability and a low excess current, which needs high crystal quality. For the measurements, mesa diodes with an active area of (50μm)² were defined by standard contact lithography and lift-off process. The samples were annealed after growth for 1min at 650°C in a forming gas atmosphere, to remove point defects formed during the low temperature MBE growth.

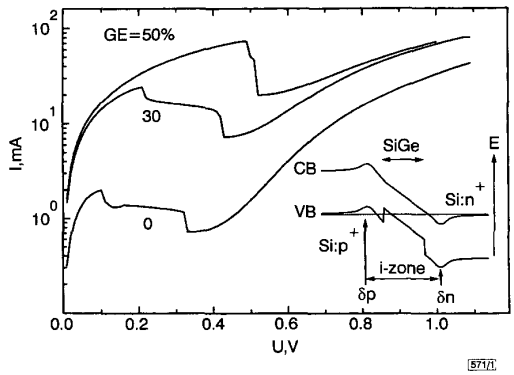

Fig. 1 *RT I–V characteristics for diodes with 0, 30 and 50% Ge within i-zone*

Inset: Schematic band structure

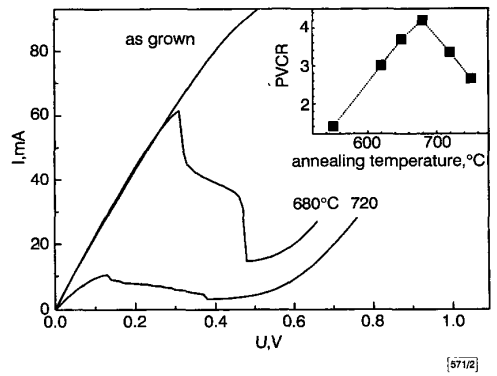

Fig. 2 *RT I–V characteristics for sample with 50% Ge for different annealing temperatures of 680°C and 720°C compared to as grown structure*

Inset: PVCR for different annealing temperatures

Fig. 1 shows the *I–V* characteristics of samples with different Ge concentrations of 0, 30 and 50% in the i-zone. The effects of Ge incorporation are a reduced B diffusion, and an additional VB offset as indicated in the inset of Fig. 1. This offset causes a more defined and thinner tunnelling barrier than the diffusion-limited δ doping layers, giving rise to an increased tunnelling probability. The shift of the peak and valley voltages to higher values with increasing current is caused by a serial resistance within the measurement setup. A pronounced increase in the peak current density from ~80A/cm² for pure Si to ~3kA/cm² for the sample with a Ge content of 50% is observed. The PVCR also shows an increase